GEOCHEMISTRY

Trace metal stoichiometry of dissolved organic matter in the Amazon plume

Martha Gledhill[1]*, Adrienne Hollister[2], Michael Seidel[3], Kechen Zhu[1]†, Eric P. Achterberg[1], Thorsten Dittmar[3,4], Andrea Koschinsky[3]

Dissolved organic matter (DOM) is a distinct component of Earth's hydrosphere and provides a link between the biogeochemical cycles of carbon, nutrients, and trace metals (TMs). Binding of TMs to DOM is thought to result in a TM pool with DOM-like biogeochemistry. Here, we determined elemental stoichiometries of aluminum, iron, copper, nickel, zinc, cobalt, and manganese associated with a fraction of the DOM pool isolated by solid-phase extraction at ambient pH ($DOM_{SPE\text{-}amb}$) from the Amazon plume. We found that the rank order of TM stoichiometry within the $DOM_{SPE\text{-}amb}$ fraction was underpinned by the chemical periodicity of the TM. Furthermore, the removal of the $TM_{SPE\text{-}amb}$ pool at low salinity was related to the chemical hardness of the TM ion. Thus, the biogeochemistry of TMs bound to the $DOM_{SPE\text{-}amb}$ component in the Amazon plume was determined by the chemical nature of the TM and not by that of the $DOM_{SPE\text{-}amb}$.

INTRODUCTION

Marine dissolved organic matter (DOM) forms a major reservoir of carbon (C), equivalent in size to that of atmospheric C (*1*). The biogeochemical cycle of marine DOM involves transfer of fixed C from the surface to the deep ocean by mixing and watermass subduction and contributes approximately 20% of the oceanic C export (*2*, *3*). Along with C, the DOM pool also contains other heteroatoms including nitrogen (N), phosphorus (P), sulfur (S) and oxygen (O), and cations such as trace metals (TMs). Important information about the geochemical cycles of elements associated with DOM can be inferred from knowledge of elemental stoichiometry and the factors influencing stoichiometry; nevertheless, only the stoichiometry of N and P in DOM have been extensively studied [e.g., (*4*)], and the elemental stoichiometries of S and TMs in marine DOM have only rarely been reported (*5*, *6*).

The TM-DOM pool, or specific components of the pool, are considered to play an important role in TM cycling, with the biogeochemical cycles of iron (Fe) (*7*, *8*), copper (Cu) (*9*–*11*), zinc (Zn) (*12*, *13*), nickel (Ni) (*10*, *11*), cobalt (Co) (*14*–*16*), and manganese (Mn) (*17*) all thought to be influenced to varying extents by binding to DOM. For Fe, binding to DOM competes with hydrolysis that would otherwise result in Fe precipitation above extremely low dissolved Fe concentrations (ca. 0.01 nM Fe at salinity 35, pH 8, and 25°C) (*18*, *19*) and thereby increases the overall inventory of this limiting nutrient in the ocean. TMs (with the notable exception of mercury) are coordinated to DOM rather than covalently bound, and binding of TMs to organic matter and adsorption of TMs onto particles can be thus expected to be influenced by the underlying chemical nature of the metal and the ligand as determined by periodic trends in their properties such as valency and ionic radius (*20*–*22*). Recent evidence suggests that the abundance of Cu, Ni, and Co relative to C that is associated with DOM in estuaries could follow the Irving-Williams series (Cu > Ni > Co) (*6*) that empirically ranks the relative affinities of divalent ions of the first-row TMs for chemically hard ligands (e.g., those containing -OH groups) and is underpinned by changes in cationic radii and the Jahn-Teller effect (*20*). The ranking of TM stoichiometry according to the Irving-Williams series in DOM suggests that metals compete for DOM-binding sites, a factor which is rarely considered during investigations of TM binding to DOM in seawaters. Furthermore, the abundance and stoichiometry of TMs bound to DOM are subject to the influence of changes in the physicochemical state of the solvating water. In estuaries, which are subject to steep gradients in physicochemical properties, including ionic strength, temperature, and pH, the binding of TMs to DOM is thought to be an important factor influencing the fluxes of TMs from the river to the sea. The binding of TMs to DOM is often assumed to mitigate against loss of TMs, resulting from flocculation or increased adsorption onto settling particles at low salinities (<5) (*23*, *24*). Such a mechanism assumes that the fraction of TMs bound to DOM does not flocculate or adsorb onto settling particles as efficiently as the fraction not bound to DOM. Nevertheless, it has been shown that removal of a portion of the DOM pool is closely coupled to Fe removal (*25*, *26*) that, in turn, suggests that binding of DOM does not mitigate against estuarine removal of TMs in all cases. There is thus uncertainty with respect to the mechanisms that govern the transport of TMs bound to DOM through the estuaries, which, in turn, influences the overall flux of TMs from river to ocean.

The Amazon estuary forms a conduit for the largest river on Earth in terms of discharge volume and creates an estuarine plume that can be traced to the center of the Atlantic Ocean (*27*). The estuarine plume is unusual in that the high flux of fresh water (100,200 to 240,000 $m^3\ s^{-1}$) (*28*) pushes the estuary onto the continental shelf, delivering DOM (*29*) and TMs (*30*–*32*) to coastal and offshore waters. The plume thus constitutes a source of nutrients (*28*) and essential TMs such as Fe, Mn, and Co to the equatorial Atlantic Ocean (*33*, *34*). Furthermore, notable recent intensification of the hydrological cycle of the Amazon River (*28*) could have consequences for the flux of TMs from the river to the equatorial Atlantic Ocean. Nevertheless, the concentrations of TMs are modified by processes

[1]GEOMAR Helmholtz Centre for Ocean Research Kiel, Kiel, Germany. [2]Department of Physics and Earth Sciences, Jacobs University Bremen gGmbH, Campus Ring 1, 28759 Bremen, Germany. [3]Institute for Chemistry and Biology of the Marine Environment, University of Oldenburg, Carl-von-Ossietzky-Str. 9-11, 26129 Oldenburg, Germany. [4]Helmholtz Institute for Functional Marine Biodiversity, University of Oldenburg (HIFMB), 26129 Oldenburg, Germany.
*Corresponding author. Email: mgledhill@geomar.de
†Present address: Department of Ocean Science and Engineering, Southern University of Science and Technology, Shenzhen, China.

occurring in the inner (salinity < 15) and outer (15 < salinity < 35) parts of the estuary, which will affect both the chemical form and quantity of elements delivered to the open ocean, and binding to DOM is an important potential modifier of these processes (*35*).

In this study, we examined the distribution of nine elements bound to DOM in the Amazon estuary, on the northwest Brazilian Shelf and in the adjacent surface waters of the North Brazil Current (NBC; Fig. 1). We compare trends in concentrations of S, P, aluminum (Al), Fe, Cu, Zn, Ni, Co, and Mn in a DOM fraction isolated by solid-phase extraction (SPE) at ambient pH ($DOM_{SPE\text{-}amb}$) from filtered (<0.2 μm) surface water samples. We quantified elements and further separated our $DOM_{SPE\text{-}amb}$ fraction by size and hydrophobicity using high-performance reverse-phase liquid chromatography (RPLC) and size exclusion chromatography (SEC), coupled to inductively coupled plasma mass spectrometry (ICP-MS). In parallel to ICP-MS analysis, we characterized the molecular and spectrophotometric properties of the DOM associated with the elements via detection of ultraviolet-visible light absorption followed by high-resolution electrospray ionization mass spectrometry (ESI-MS). We assess trends in TM stoichiometry relative to C (C:TM) in the plume and relate them to the chemical periodicity of the metal and stoichiometries predicted by a nonideal competitive adsorption (NICA) model (*36*). We use the observed trends to identify key TM properties that influence binding of TMs to DOM and the biogeochemical behavior of the TM-DOM fraction in the Amazon plume.

RESULTS AND DISCUSSION

Elemental composition of $DOM_{SPE\text{-}amb}$ in the Amazon plume

Our study took place during the wet season in April to May 2018 when riverine flow in the lower Amazon River typically approaches its maximum of 200,000 to 250,000 $m^3\ s^{-1}$ (*28*). The distribution of surface water salinity in the study area, interpolated from data acquired with the ship's underway system (cruise track in fig. S1), showed that the Amazon plume flowed in a north-westerly direction and was largely constrained to the shelf. The inner estuary with surface water salinities <15 was characterized by depths of ≤25 m (Fig. 1). In this part of the estuary, dissolved inorganic P (DIP) concentrations decreased, while pH and chlorophyll a increased (Fig. 2, A to C) as the estuarine waters transitioned from the turbid, light limited waters of the estuarine mixing zone (S < 7, depth < 17 m, chlorophyll a ≤ 1 μg $liter^{-1}$) to higher–chlorophyll a (3 to 13 μg $liter^{-1}$), nutrient-depleted waters. Fluctuations in concentrations of DIP and pH in the inner estuary could therefore be largely explained by changes in phytoplankton productivity. In the outer estuary (15 < S < 35), we observed the highest chlorophyll a concentration (27.5 μg $liter^{-1}$), and DIP was variable although consistently <0.2 μM, suggesting that a dynamic DIP cycle likely influenced by a reported large sedimentary flux of DIP at the time (*37*) and high phytoplankton biomass in the plume (Fig. 2C). There was an input of DIP to surface waters adjacent to the mangrove forest (Fig. 2C; S = 27.6), but this was rapidly depleted in an offshore direction by phytoplankton productivity. Sediments associated with mangrove forests have been identified as a source of dissolved organic carbon (DOC) (*30*, *38*), inorganic C (*39*), and TMs (*30*, *31*) to coastal waters in this region. DOC concentrations (Fig. 2D) agreed with those reported in the region (*29*) and showed some evidence of removal in the inner estuary and inputs close to the mangrove forests [see also (*30*)], but the considerable changes in chlorophyll a in the estuarine plume did not appear to have a marked impact on the DOC concentrations.

We concentrated DOM and elements ($S_{SPE\text{-}amb}$, $P_{SPE\text{-}amb}$, $Fe_{SPE\text{-}amb}$, $Al_{SPE\text{-}amb}$, $Cu_{SPE\text{-}amb}$, $Zn_{SPE\text{-}amb}$, $Ni_{SPE\text{-}amb}$, $Co_{SPE\text{-}amb}$, and $Mn_{SPE\text{-}amb}$) using SPE at ambient pH to minimize potential changes in extracted $TM_{SPE\text{-}amb}$ stoichiometry that could arise from sample acidification,

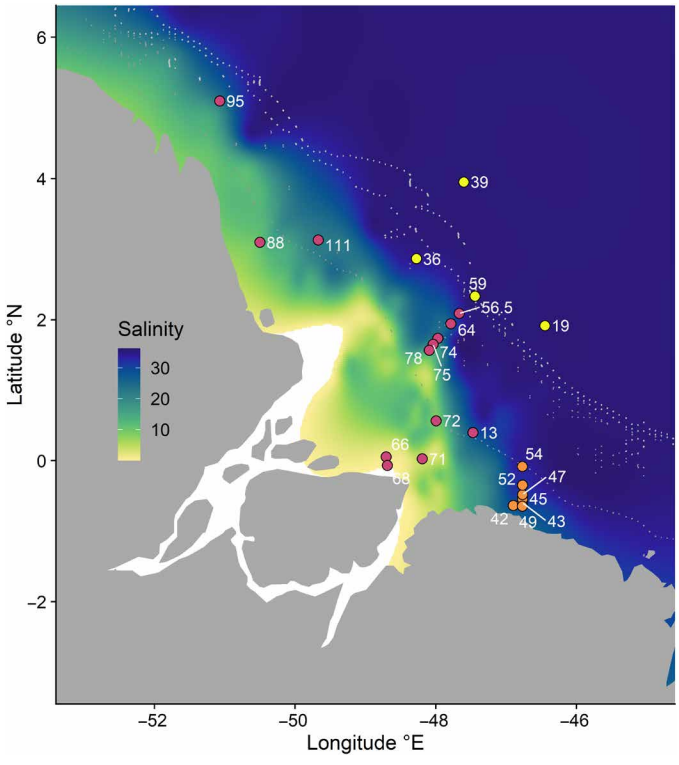

Fig. 1. Map of the study area showing sampling sites. Depth contours are for 25, 200, and 1000 m. Symbol colors indicate samples collected in the estuary (red), southwest of the estuary off a belt of mangrove forests (orange), and in the North Brazil Current (yellow). Labels show station numbers. Salinity was interpolated from data recorded using the ship's underway system. For cruise track, see fig. S1.

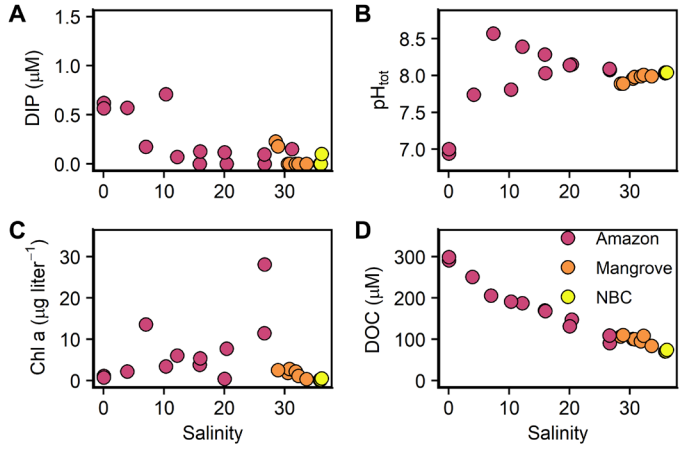

Fig. 2. Biogeochemical characteristics of the study area. Variation in (**A**) DIP, (**B**) pH (expressed on the total scale), (**C**) chlorophyll a (chl a), and (**D**) DOC with salinity in the study area. Colors show samples collected in the estuary (red), southwest of the estuary off a belt of mangrove forests (orange), and in the North Brazil Current (yellow).

which is typically used to improve DOM recoveries (*40*). We found a relatively constant but low recovery of 8 ± 2% for $C_{SPE\text{-}amb}$ (n = 22) in our extracts (*30*), which is comparable to recoveries obtained using SPE at pH 8 in other studies (*6*, *41*). We calculated the total concentrations of elements concentrated from the sum of all peaks detected in each chromatographic mode, SEC (Fig. 3) and RPLC (fig. S2). We determined the relative abundance of the DOM component via summing peaks obtained by either ultraviolet absorbance at 254 nm (A_{254}) or ion abundances obtained in negative and positive electrospray ionization modes ($EICneg_{SPE\text{-}amb}$ and $EICpos_{SPE\text{-}amb}$). All parameters showed a decrease from the Amazon riverine end-member to the NBC marine end-member (Fig. 3 and fig. S2). Comparison of results obtained by SEC and RPLC showed good agreement with respect to trends between the two chromatographic modes (fig. S3 and table S1). Our values for $S_{SPE\text{-}amb}$, $P_{SPE\text{-}amb}$, $Cu_{SPE\text{-}amb}$, $Ni_{SPE\text{-}amb}$, and $Co_{SPE\text{-}amb}$ are within the range of values reported for marine waters (Table 1) (*5*, *6*, *11*). Concentrations of $P_{SPE\text{-}amb}$ were considerably lower than dissolved organic P typically observed in estuaries and coastal waters following wet oxidation techniques (*42*, *43*), as expected given the percentage DOC recovery obtained for our study. To our knowledge, there have been no reports of total concentrations of $Fe_{SPE\text{-}amb}$, $Al_{SPE\text{-}amb}$, $Mn_{SPE\text{-}amb}$, and $Zn_{SPE\text{-}amb}$. Concentrations of $Fe_{SPE\text{-}amb}$ in the marine end-member (0.12 ± 0.03 nM) were an order of magnitude higher than the highest siderophore concentrations reported in the ocean (*44*). We further highlight that recoveries of siderophores are typically higher [46%; (*44*)] than the average recovery observed for DOC in this study, and siderophores may therefore make up a minor component of the total organically bound Fe fraction in coastal waters (*45*).

All parameters behaved nonconservatively with respect to salinity. Removal at low salinities was observed for all elements but was weakest for $C_{SPE\text{-}amb}$ and $Cu_{SPE\text{-}amb}$ (49 ± 3% and 46 ± 8% removal respectively), and strongest for $Fe_{SPE\text{-}amb}$ and $Al_{SPE\text{-}amb}$ (94 ± 1% and 93 ± 4% respectively, table S2). There was some evidence for an outer-estuary increase in $P_{SPE\text{-}amb}$, $Zn_{SPE\text{-}amb}$, and $Ni_{SPE\text{-}amb}$ at salinities between 15 and 30. Concentrations of $S_{SPE\text{-}amb}$ and $P_{SPE\text{-}amb}$ offshore from the mangrove forests were similar to those observed in the riverine end-member, while $A_{254SPE\text{-}amb}$, $Cu_{SPE\text{-}amb}$, $Zn_{SPE\text{-}amb}$, $Co_{SPE\text{-}amb}$, and $Ni_{SPE\text{-}amb}$ were slightly elevated close to the mangrove forests, possibly as a result of inputs from the organic carbon–rich mangrove sediment pore waters (*46*). The NBC showed elevated concentrations of $S_{SPE\text{-}amb}$, $P_{SPE\text{-}amb}$, and $Zn_{SPE\text{-}amb}$ but lower concentrations of Fe compared to high-salinity estuarine samples (Fig. 3).

We compared $TM_{SPE\text{-}amb}$ with dissolved TM concentrations by assuming that the 8% recovery observed for $C_{SPE\text{-}amb}$ (*30*) was also representative for the $TM_{SPE\text{-}amb}$ pool (Fig. 4). Extrapolated Fe, Cu, Zn, and Co concentrations were similar to those for the dissolved TMs, while extrapolated Al, Ni, and Mn concentrations were consistently lower than the dissolved TM concentrations. This approach represents a first-order estimate, because we do not know the TM concentrations associated with the DOM that was not extracted under our conditions, but our results are consistent with previous estimations of ligand concentrations in estuarine waters, which have been shown to be close or in excess to dissolved TM concentrations

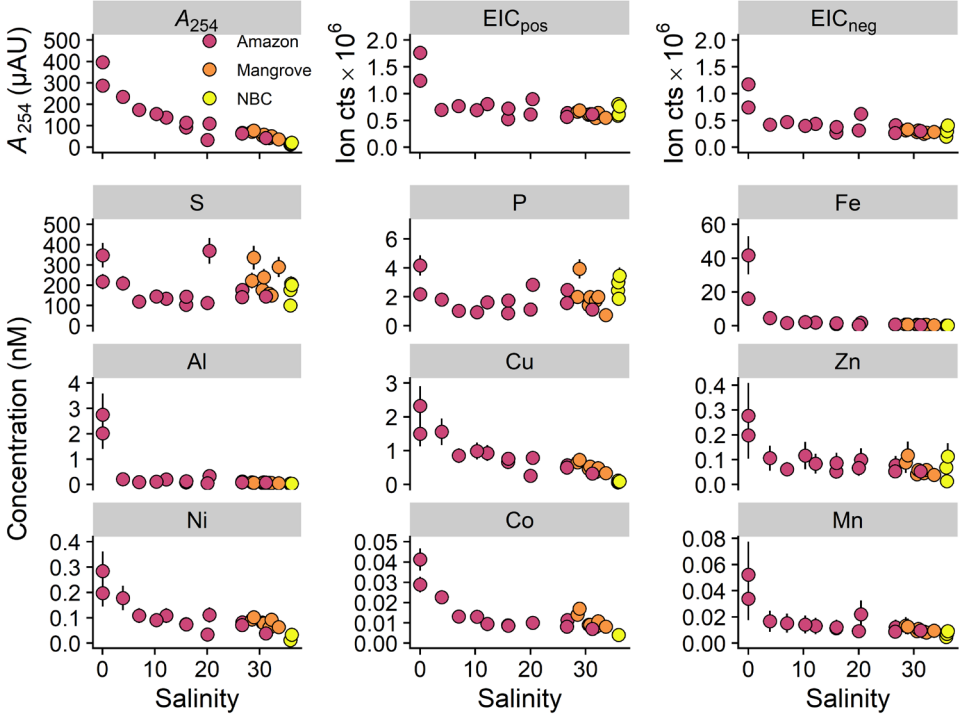

Fig. 3. Relationship between $DOM_{SPE\text{-}amb}$ components and salinity in the study area. Salinity-property plots are shown for ultraviolet absorbance at 254 nm (A_{254}), ion abundances in positive and negative ionization modes (EICpos and EICneg, respectively), and total concentrations of elements determined in $DOM_{SPE\text{-}amb}$ samples collected in our study area (parameter identity is indicated in the facet heading). Results shown here were calculated from the sum of the peak areas observed in SEC data. Vertical bars represent the analytical uncertainty associated with element concentrations. Colors show samples collected in the estuary (red), southwest of the estuary off a belt of mangrove forests (orange), and in the North Brazil Current (yellow). μAU, micro–arbitrary units.

Table 1. Total end-member concentrations (or ion counts for ESI-MS) observed on SEC and RPLC analysis of $DOM_{SPE\text{-}amb}$ in the Amazon River and NBC. ND, not determined. HPLC, high-performance liquid chromatography.

Element	$DOM_{SPE\text{-}amb}$ concentration (nM), riverine end-member ($n = 1$)		$DOM_{SPE\text{-}amb}$ concentration (nM), marine end-member ($n = 3$)		Literature values for $DOM_{SPE\text{-}amb}$ element concentrations determined by HPLC–ICP-MS
	SEC	RPLC	SEC	RPLC	
Al	2.8	2.7	0.020 ± 0.001	0.11 ± 0.09	
Co	0.04	0.17	0.004	0.012 ± 0.003	0.02–0.07 (Elbe) (*6*)
Cu	2.3	1.4	0.07 ± 0.02	0.08 ± 0.03	1.4–4.3 (Elbe) (*6*) 0.045–0.15 (South East Pacific) (*11*)
Fe	42	9.5	0.08 ± 0.03	0.044 ± 0.039	
Mn	0.05	0.03	0.005	0.002 ± 0.001	
Ni	0.28	0.25	0.02 ± 0.01	0.008	0.09–0.44 (Elbe) 0.025–0.05 (South East Pacific) (*11*)
P	4.2	1.9	2.5 ± 0.8	1.6 ± 0.3	5.2–12.4 (Elbe) (*6*)
S	350	161	168 ± 60	24 ± 3	~100 (Atlantic Ocean) (*5*) 190–350 (Elbe) (*6*)
Zn	0.2	0.32	0.07 ± 0.05	ND	
ElCpos	1.76×10^6	3.27×10^5	$0.65 \pm 0.09 \times 10^6$	$0.44 \pm 0.1 \times 10^5$	
ElCneg	1.18×10^6	6.86×10^5	$0.3 \pm 0.1 \times 10^6$	$0.65 \pm 0.2 \times 10^5$	

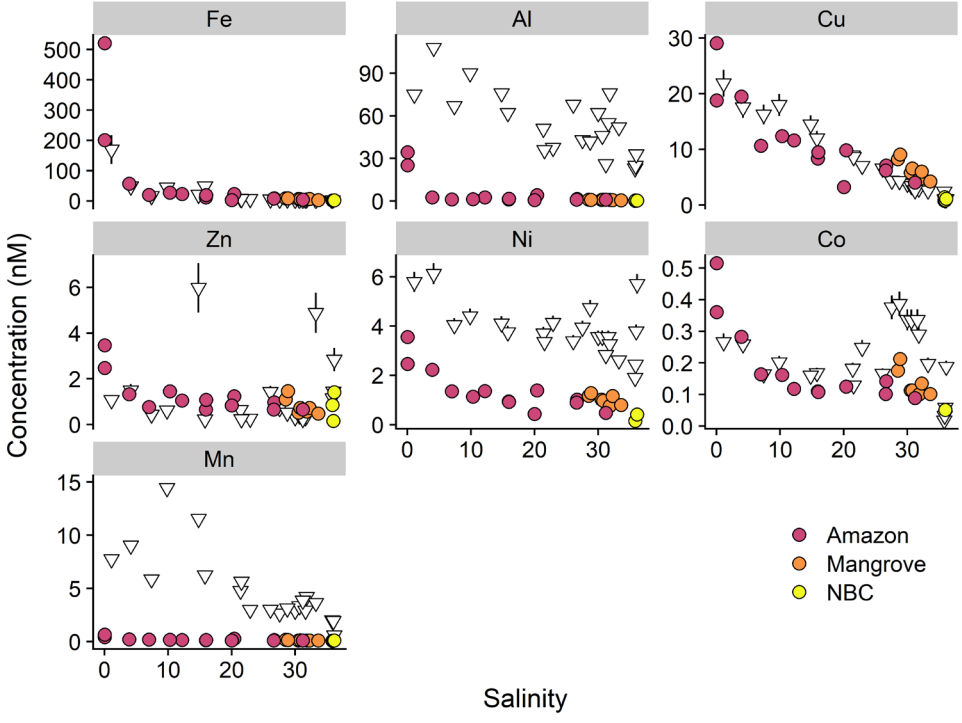

Fig. 4. Estuarine behavior of TMs associated with $DOM_{SPE\text{-}amb}$ compared to observed dissolved (<0.2 μm) TM concentrations. $TM_{SPE\text{-}amb}$ is shown as filled circles colored according to sample origin, and dissolved TM concentrations are shown as open triangles. Here, we assume that TMs bound to DOM were extracted with the same efficiency as determined for DOC (8 ± 2%). Concentrations of TMs determined in $DOM_{SPE\text{-}amb}$ were therefore multiplied by a factor of 12.5 for this comparison. Dissolved TM concentrations are those for samples collected from surface waters in close proximity to $DOM_{SPE\text{-}amb}$ samples (see fig. S1). We show $TM_{SPE\text{-}amb}$ values obtained on analysis by SEC. Vertical bars represent analytical uncertainties associated with dissolved trace element concentrations. Uncertainties associated with the $TM_{SPE\text{-}amb}$ fraction are omitted for clarity.

for Cu, Fe, and Zn (*10*, *13*, *47*–*49*), but lower than dissolved Ni (*10*, *50*, *51*) (to our knowledge, no equivalent data is available for Co, Al, or Mn). With the exception of Al and Mn, the relative change in concentrations of both dissolved and $TM_{SPE\text{-}amb}$ in the plume appeared to be well coupled. While we cannot rule out differences in extraction efficiencies between TMs bound to DOM, our results suggest that the extraction efficiency of TMs by SPE at ambient pH is strongly linked to the overall poor retention of DOM, which, in turn, reflects the hydrophilic nature of DOM at ambient pH.

Elemental stoichiometry of $DOM_{SPE\text{-}amb}$

Examination of the chromatographic (Supplementary Text, figs. S4 to S6, and tables S3 and S4) and molecular properties (Supplementary Text, fig. S7, and table S5) showed that not all the chromatographic fractions associated with $DOM_{SPE\text{-}amb}$ had molecular and spectrophotometric characteristics typically associated with bulk DOM [e.g., (*29*, *52*)]. We found that A_{254} and ion counts observed by ESI-MS were most abundant in a medium–molecular weight (MMW) fraction (0.5 < MMW < 10 kDa; Supplementary Text and fig. S4) and a hydrophobic (Hphob) fraction (fig. S5). Furthermore, molecular signatures observed by ESI-MS in these two fractions were similar to those observed for DOM preconcentrated by SPE at pH 2 in the Amazon plume (Supplementary Text) (*29*). In contrast, the absorbance and molecular signatures for the low molecular weight, the high–molecular weight (HMW), and the hydrophilic (Hphil) fractions suggested that they were not representative of DOM (Supplementary Text, figs. S4 to S6, and table S3 and S4). We therefore estimate elemental stoichiometries for $DOM_{SPE\text{-}amb}$ from the concentrations of TMs determined for the Hphob and MMW fractions (Table 2 and Fig. 5). We estimated C concentrations associated with MMW and Hphob fractions from the relationship between A_{254} and $C_{SPE\text{-}amb}$ and expressed our stoichiometries as C:element ratios [see Materials and Methods and (*5*, *53*)].

Ratios determined for the heteroatoms S and P in $DOM_{SPE\text{-}amb}$ were similar to those reported for the Elbe estuary in the northwest Europe (Table 2) (*6*). Sulfur ratios were within the range reported for phytoplankton (Table 2) (*54*), which could point to a biological source for S in $DOM_{SPE\text{-}amb}$ (*5*), although abiotic sulfurization of DOM has also been shown to be important in marine waters (*55*). In contrast, P ratios were higher in $DOM_{SPE\text{-}amb}$ compared to the Redfield ratio of 106, as is typical for marine DOM (*56*). Our marine end-member P ratios were lower than those observed for surface organic matter (374 mol mol^{-1}) (*56*) and the Amazon River (550 mol mol^{-1}) (*57*) but comparable to ratios observed for recalcitrant organic matter in the deep ocean (3511 mol mol^{-1}) (*56*). For TMs, our ratios were similar to those observed in the Elbe estuary (Table 2) (*6*). The C:Fe and C:Cu ratios observed in HMW and Hphob fractions were in a similar range to those reported for Suwannee River natural organic matter, and our ratios for Ni, Zn, and Mn were higher than the reported values (Table 2) (*58*). Carbon:Fe ratios observed in the MMW fraction of the riverine end-member were within range of values for Suwannee River humic and fulvic acids (900 to 2200 mol mol^{-1}) (*26*, *59*, *60*). Overall, our comparison with literature values shows that the number of reported values for C:TM stoichiometry in both riverine and marine natural organic matter is still limited, but there appears to be a consistency in their magnitude between different types of organic matter in the various studies.

We estimated the relative abundance of molecules containing elements determined in our study from the average molecular weight (ca. 400 Da; table S5) and the average number of C atoms observed for molecular formulas in MMW and Hphob peak fractions (ca. 20; table S5). Assuming that only one atom of an element is incorporated into any given molecule, we estimate that approximately 1 in every 5 to 10 $DOM_{SPE\text{-}amb}$ molecules contains an S atom; 1 in every 100 to 1000 molecules contains a P atom; 1 in every 1000 to 10,000 molecules contains an Al, Fe, or Cu ion; while Zn, Ni, and Co would be present in approximately 1 in every 100,000 molecules, and Mn would be present in 1 in every 1 million molecules. It should be emphasized that these estimates are very broad and do not consider bias in ESI-MS ionization efficiency, which has been shown to vary with molecular properties including basicity, molecular volume, and hydrophobicity (*61*), and can also all be altered by the presence of heteroatoms or metal ions. Furthermore, the number of elemental atoms or ions in a molecule could be greater than 1. Nevertheless, the estimates of the relative number of molecules containing P and S are comparable to the relative numbers of S and P containing molecular formula (ca. 20 to 30% and 1 to 5%, respectively) detected by Fourier-transform ion cyclotron resonance (FT-ICR)-MS (*55*, *62*) in marine DOM. In our study, we did not include S or P as possible elements in formula assignment because we resolved masses to 3 parts per million (ppm) during chromatographic peak detection. Our estimates of the relative abundance of molecules containing TMs are consistent with the lack of detected TM containing molecular ions in our study, as well as the detection of low numbers of molecular formula containing TM ions in DOM by FT-ICR-MS (*41*), because (assuming similar ionisation efficiencies) even for Fe, Al, or Cu, we could expect only very few molecular formulae for these elements given our detection of ca. 4000 to 5000 individual features. Furthermore, because proton-binding site concentrations of ca. 0.1 mol mol^{-1} C have been reported (*63*, *64*), which would lead to an average of two available protonation sites per molecule, it is also clear that TMs occupy a limited number of the total available number of binding sites, likely because only a limited number of the molecular isomers have structures favorable for metal chelation.

Stoichiometry and behavior of TMs bound to organic matter is underpinned by chemical periodicity of the TM

The stoichiometries of the TMs in the MMW and Hphob fraction increased in the order Fe ≈ Cu < Al < Zn ≈ Ni < Co < Mn (Fig. 5). The rank order of the C:TM stoichiometries in these fractions is not the same as that observed for ratios of DOC to total dissolved metal concentration (Al < Fe ≈ Mn ≈ Ni ≈ Cu ≈ Zn < Co), which reflects the relative abundances of the TMs in the study area. The rank order of observed C:TM stoichiometries in MMW and Hphob fractions also does not reflect those observed in phytoplankton (Fe ≈ Zn < Mn ≈ Ni ≈ Cu < Co;), which are determined by phytoplankton TM requirements (*54*, *65*). The rank order of C:TM stoichiometries was thus unique to the Hphob and MMW $DOM_{SPE\text{-}amb}$ fractions. For the divalent TMs (Cu, Zn, Ni, Co, and Mn), the rank order followed the Irving-William's series, as has been reported for Cu, Ni, and Co in the $DOM_{SPE\text{-}amb}$ fraction in the Elbe estuary (*6*). Extension of the Irving-Williams series beyond the divalent first-row transition elements is not possible because shielding effects from changes in the ionic charge and number and type of electron orbitals also affect ionic radii. However, comparison of our determined C:TM stoichiometries with the thermodynamic stability constants of 1:1 metal complexes with chemically hard anions including the hydroxide anion, EDTA, nitrilotriacetic acid, and 4-sulfocatechol showed that C:Fe and C:Al ratios follow a trend consistent with the increase in

Table 2. Element stoichiometry for MMW and Hphob peaks. Values are expressed as mol C mol^{-1} element. For Zn, only values for MMW are shown because the Zn Hphob and Hphil peaks could not be separated. Uncertainties are expressed as the range ($n = 2$) or ±1 SD ($n > 2$) for each region of the study area. Also shown in this table are literature values for the Elbe estuary, phytoplankton, and Suwannee River fulvic acid. NA, not applicable.

	DOM fraction	S	P (×10^3)	Al (×10^3)	Fe (×10^3)	Cu (×10^3)	Zn (×10^5)	Ni (×10^5)	Co (×10^5)	Mn (×10^5)	Reference
Riverine end-member ($n = 2$)	MMW	130 ± 20	12 ± 5	17 ± 8	2.2 ± 0.2	20 ± 2	1.8 ± 0.5	1.6 ± 0.1	10.6 ± 0.1	30 ± 4	This study
	Hphob	300 ± 20	29	20 ± 8	16 ± 16	30 ± 22	ND	2.2	7.6 ± 6.5	21 ± 7	This study
Estuary ($n = 11$)	MMW	110 ± 40	11 ± 5	150 ± 50	20 ± 10	23 ± 5	2.4 ± 0.5	1.9 ± 0.4	15 ± 3	46 ± 9	This study
	Hphob	390 ± 51	22 ± 13	120 ± 30	102 ± 60	34 ± 7	ND	7.7 ± 7.3	11 ± 3	46 ± 25	This study
Mangrove ($n = 7$)	MMW	50 ± 10	11 ± 5	180 ± 30	27 ± 8	23 ± 4	2.1 ± 0.4	1.4 ± 0.2	11 ± 2	42 ± 11	This study
	Hphob	310 ± 60	10 ± 3	110 ± 20	127 ± 80	32 ± 6	ND	3.6 ± 1.8	8 ± 2	39 ± 20	This study
NBC ($n = 4$)	MMW	360 ± 7	2.3 ± 0.5	270 ± 70	69 ± 20	74 ± 13	0.9 ± 0.3	2.9 ± 0.1	14	63	This study
	Hphob	250 ± 90	3.5 ± 0.7	70 ± 30	182 ± 70	70 ± 11	ND		4.8 ± 1.4	30 ± 10	This study
Elbe estuary riverine end-member	Total	107	8.2	ND	ND	31	ND	27	5.6	ND	(*6*)
Elbe estuary marine end-member	Total	163	2.9	ND	ND	40	ND	2.3	10	ND	(*6*)
Phytoplankton	NA	95	0.124	ND	16.5	326	1.6	ND	6.5	ND	(*54*)
Suwannee River natural organic matter	Total	ND	ND	ND	1.6	39	0.23	0.6	ND	2.6	(*58*)

binding strengths observed for ligands containing chemically hard functional groups (Fig. 6A and fig. S8). The rank order of observed C:TM stoichiometries therefore supports the hypothesis that metals compete for binding sites within the heterogeneous $DOM_{SPE\text{-}amb}$ pool. Furthermore, the correspondence of our C:TM ranking with stabilities of hard anions points to a likely predominant role for phenolic or carboxylic groups in TM binding by marine DOM (*66*).

We therefore compared our observed C:TM stoichiometry in MMW and Hphob peak fractions to those predicted for the total marine DOM pool with a competitive binding model (*67*). We used the NICA-Donnan model (*19*, *68*) in combination with bulk DOC concentrations, ambient pH, dissolved TM concentrations, NICA affinity and nonideality parameters (table S7), and major element concentrations derived from conservative mixing of Amazon River water with seawater (Supplementary Text). We accounted for potential oversaturation of Fe^{3+} with respect to $Fe(OH)_3(s)$ by allowing for formation of insoluble Fe hydroxide [$Fe(OH)_3(s)$] in our calculations (*19*). Predicted C:TM ratios were within an order of magnitude of observed values for all TMs (Fig. 5 and fig. S9). Closer examination of the trends with salinity showed a better agreement between predicted and observed values for C:Fe, Al, and Ni ratios throughout the plume, while predicted C:Mn, Zn, Cu, and Co deviated from observations at low salinity (Cu and Mn), mid salinities (Zn), or high salinity (Co) (fig. S9). Deviations likely arise because the speciation calculations do not incorporate all processes for all TMs, and because of limited availability of NICA parameters that describe TM binding to marine DOM. For example, with the exception of Fe, where formation of $Fe(OH)_3(s)$ plays a key role in determining the calculated C:Fe ratio, our calculations do not consider biogeochemical mechanisms such as scavenging onto particles, or the presence of a highly dynamic colloidal fraction, that are known to strongly influence TMs in the inner estuary. The Amazon River carries a high sediment load (ca. 1×10^8 t $month^{-1}$ in April) that largely settles out in the inner estuary above the 15-m contour (*69*). These processes might especially affect Mn, which was observed in an HMW fraction at low salinities (fig. S6) and has been shown to form inorganic colloids through microbial oxidation (*70*–*72*). Furthermore, there is limited availability of NICA parameters for marine DOM in the literature (Supplementary Text), and we therefore approximated values for our study area. We did not account for potential changes in NICA

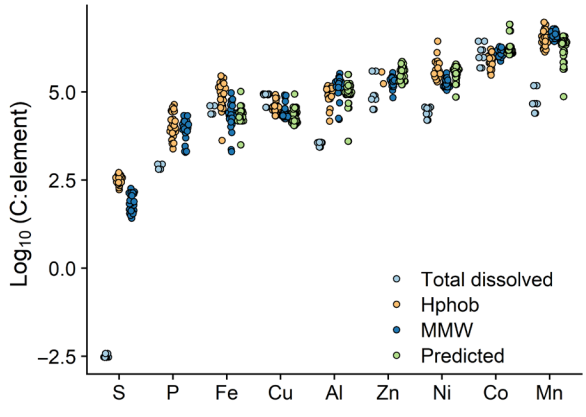

Fig. 5. Elemental stoichiometry observed in MMW and Hphob fractions. Elements are ranked on the *x* axis according to their stoichiometry in the MMW fraction. C:element ratios are plotted as $\log_{10}$ values using a quasi-random density plot. "Total dissolved" points show the ratio calculated for dissolved elements to DOC using concentrations of S as sulphate (calculated from salinity), DIP, and total dissolved TM concentrations. Predicted values were obtained from calculations of TM speciation at ambient salinity, pH, and dissolved TM and DOC concentrations, assuming that binding sites in DOM scale to DOC. We assumed that TM-DOM binding could be represented by the NICA model combined with the Donnan model for electrostatic interactions. For calculations of C:Fe ratios, we assumed competition between NICA binding sites and the formation of $Fe(OH)_3(s)$ (*19*).

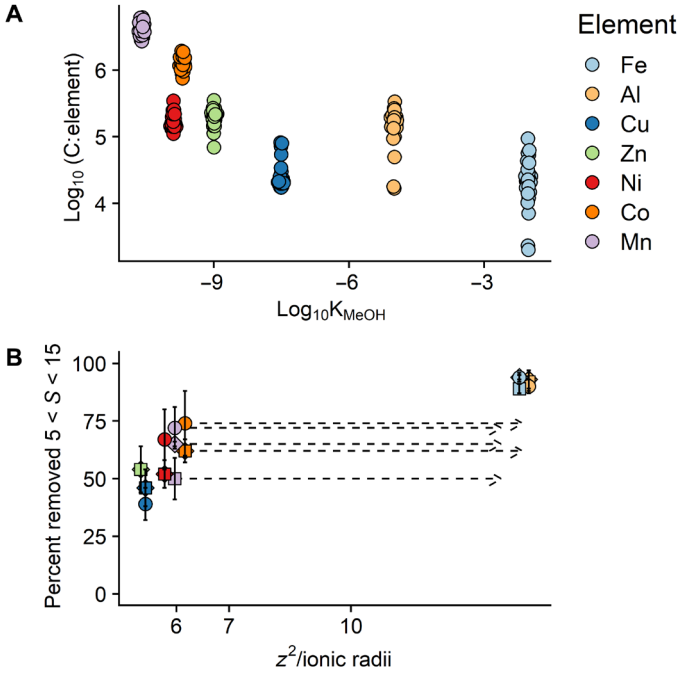

Fig. 6. Influence of chemical periodicity on $TM_{SPE\text{-}DOM}$ biogeochemistry in the Amazon estuary. (**A**) The decrease in C:TM ratios (circles show $\log_{10}$ values for the MMW fraction as a quasi-random density plot) is consistent with trends in other thermodynamic stability constants of metal complexes as illustrated here for first hydrolysis constant ($\log_{10}K_{MeOH}$). Cu, Co, and Mn were assumed to be present in the +2 oxidation state, while Fe was assumed to be in the +3 oxidation state. (**B**) The proportion of $TM_{SPE\text{-}amb}$ fraction that is removed at low salinity increased with polarizing power of the TM ion as expressed by the square of the oxidation state (z^2) divided by Shannon's ionic radii. Diamond symbols show the percentage removed for the total $TM_{SPE\text{-}amb}$ concentrations determined by SEC, squares removal of the MMW fraction, and circles removal of the Hphob fraction. For Mn and Co, the dashed arrow represents the increase in polarizing power that results from oxidation from the +2 oxidation state to the +3 oxidation state. Note the $\log_{10}$ scale for polarizing power.

parameters that likely occur with changes in DOM composition and thus implicitly assume that neither the degree of heterogeneity nor the distribution of binding sites changed with salinity. However, we observed a decrease in the specific A_{254} per mg C m^{-1} ($SUVA_{254}$) from 0.83 in the Amazon River to 0.26 ± 0.03 in NBC samples (n = 4; fig. S10), and a greater loss of highly aromatic compounds and unsaturated aliphatic compounds in ESI-MS data in comparison to highly unsaturated compounds (fig. S11). The MMW and Hphob fractions therefore became less aromatic as salinity increased, and this could point to a reduction in phenolic-like binding sites as salinity increases. Furthermore, recent work suggests that heterogeneity of DOM binding sites varies in marine waters (*63*, *64*). Thus, NICA parameters likely change through our study area, although further work is required to quantify these changes.

We further examined the proportion of elements in our $DOM_{SPE\text{-}amb}$ fractions that were lost in the inner estuary when the river water endmember first mixed with higher-salinity waters (table S2 and Fig. 6B). Removal of TMs increased in the order Cu ≈ Zn ≈ Ni < Mn < Co < Fe < Al. Cu, Zn, and Ni removal were within range (43 to 52%) of both A_{254} (47 ± 1%) and $C_{SPE\text{-}amb}$ (49 ± 3%). The strong removal of $Al_{SPE\text{-}amb}$ and $Fe_{SPE\text{-}amb}$ (>90%) reflects their chemical hardness (*21*) and well-characterized tendency to hydrolyze and be scavenged within the low-salinity region of the estuary (*22*, *35*). Quantitatively, a tendency to hydrolyze can be related to the polarizing power of an ion, as defined by the square of the oxidation state divided by the Shannon ionic radii (*22*). Direct comparison confirmed that the proportion of the TM associated with the $DOM_{SPE\text{-}amb}$ fraction lost during mixing increased with polarizing power (Fig. 6B).

Both C:TM stoichiometry and the relative removal of TMs associated with $DOM_{SPE\text{-}amb}$ thus indicate that the behavior of the TMs associated with the $DOM_{SPE\text{-}amb}$ fraction in the Amazon plume is governed by the underlying ionic characteristics of the TMs. Hence, Al and Fe $DOM_{SPE\text{-}amb}$ fractions are largely removed because the chemical hardness of Al and Fe and the tendency to hydrolyze override any stabilizing effect that binding to $DOM_{SPE\text{-}amb}$ might confer. Cobalt and Mn have the next highest polarizing power and low affinities for $DOM_{SPE\text{-}amb}$ binding sites, and hence, these two metals have high C:TM stoichiometries and relatively high removal rates that are likely facilitated by microbially mediated oxidation to Co(III) and Mn(III) or Mn(IV) (*71*, *72*). Furthermore, the high C:Co and C:Mn ratios in $DOM_{SPE\text{-}amb}$ are consistent with a predominant oxidation state of +2 for these elements because the increased charge associated with higher oxidation states would be expected to result in higher affinities for DOM sites and thus lower C:Co and C:Mn ratios. On the other hand, the relatively lower removal rates of Cu, Zn, and Ni are closest to that of A_{254}, because these TMs have a low polarizing power combined with a relatively high affinity for $DOM_{SPE\text{-}amb}$ binding sites. Our results therefore indicate that binding to DOM has a variable impact on the transport and removal of individual TMs in the Amazon estuary because the biogeochemical behavior of the DOM bound fraction is governed by the same underlying chemical characteristics that govern the unbound TM.

Our study has shown that simultaneous determination of the relative abundance of a suite of TMs bound to DOM provided new insights into underlying factors controlling TM transport and TM-DOM interactions in our study region. A major uncertainty in our work is how representative our results are of bulk DOM because we only extracted ca. 8% of the total DOC pool. Nevertheless, both molecular characteristics and the agreement between C:TM stoichiometries predicted from dissolved TM and DOC concentrations and observed $C{:}TM_{SPE\text{-}amb}$ stoichiometries suggest that our results could be representative of a larger fraction of the DOM pool. We show that the concentrations of TMs bound to DOM in marine waters are consistent with competitive interactions between TMs for a heterogeneous pool of binding sites. Furthermore, we demonstrate that chemical hardness, as illustrated by the polarizing power of TMs, is an important factor in determining the fraction of TMs bound to DOM that will be removed at low salinity in an estuary. These two factors therefore provide a framework to mechanistically constrain the transport of TMs bound to DOM in estuaries. We suggest that further parameterization of the intrinsic binding properties of TMs to marine DOM will allow for improved predictions on how TM binding to DOM will change as a result of changes in hydrological cycles, riverine TM concentrations, pH, and temperature that occur as a result of climate change and further anthropogenic activities.

MATERIALS AND METHODS

Samples were collected onboard the RV *Meteor* during the M147 (GEOTRACES GApr11) process cruise in the Amazon plume and

adjacent north-eastern Brazilian Shelf in the period between 29 April and 20 May 2018 (Fig. 1). Samples for $DOM_{SPE\text{-}amb}$ were collected from surface waters (<10-m depth) using standard (Niskin, Ocean Test Equipment) or ultraclean (C-Free, Ocean Test Equipment) sampling bottles fitted with a conductivity, temperature depth (CTD) profiler (Seabird 911). Samples were filtered in-line through a 0.22-μm polyvinylidene fluoride membrane filter (Sterivex-GV, Millipore) and passed over 200-mg modified polystyrene divinyl benzene SPE column (ENV+, Biotage, Sweden) at ambient pH (*30*). A vacuum manifold was used to regulate the flow rate to approximately 10 ml min^{-1}. After removing excess water, cartridges were stored frozen at −20°C before extraction. Once defrosted at GEOMAR, cartridges were washed with 5 ml of 10 mM $(NH_4)_2CO_3$ (pH 8), and then $DOM_{SPE\text{-}amb}$ was eluted with 5 ml of 81:14:5:1 (v:v:v:v) acetonitrile:propan-2-ol:H_2O:formic acid and stored at −20°C between analysis. Concentrations of elements, light absorbance, and mass-to-charge ratios of ionizable ions in $DOM_{SPE\text{-}amb}$ were subsequently analyzed after evaporation of a 750-μl aliquot to <100 μl and adjustment of the sample pH to 6.5 with ammonium acetate. $DOM_{SPE\text{-}amb}$ fractions were separated by high-performance RPLC or by high-performance SEC coupled to a diode array detector, an inductively coupled mass spectrometer, and an electrospray ionization mass spectrometer. Further details on the instrumental setup are provided in Supplementary Text.

Elemental concentrations were standardized using thiamine (S), flavin mononucleotide (P), ferrioxamine B (Fe), cobalamin (Co), and (in a separate standard curve) complexes of Al, Co, Cu, Zn, and Mn with EDTA at pH 6.5 (10 mM ammonium acetate). EDTA was added at 20% excess of TMs in the standards. For SEC, we additionally analyzed polymer standards (polysulfonesulfate) and Suwannee River fulvic and humic acids for molecular weight comparison (*30*). Concentrations of Cu obtained on SEC analysis of $DOM_{SPE\text{-}amb}$ were presented in (*30*). Percentage analytical uncertainty for elemental concentrations in $DOM_{SPE\text{-}amb}$ determined by ICP-MS were calculated from repeated analysis of standards during the chromatographic run ($n = 6$).

We present here a subset of the total nutrient, TM, and DOC surface data obtained in the study area. Our subset is restricted to samples collected in close proximity to the $DOM_{SPE\text{-}amb}$ samples (fig. S1). The complete datasets for DOC and nutrients and the methods used for determination of TMs, nutrients, and DOC are described in detail in (*30*). The complete dataset for dissolved Cu, Ni, and Co are described in (*30*, *31*).

For analysis of $C_{SPE\text{-}amb}$ in extracts, solvents were first removed by evaporation and residual organic matter redissolved in 0.1 M HCl before analysis. We used the relationship between $C_{SPE\text{-}amb}$ in extracts and A_{254} to obtain the proportion of C associated with each peak fraction observed in chromatograms. Deep-sea reference samples (University of Miami, USA) were analyzed alongside samples for quality control.

We used the software program ORCHESTRA (*73*) to calculate C:TM ratios for DOM in the Amazon plume, assuming that DOM has binding properties that are similar to fulvic acids and binding sites scale to DOC concentrations (*19*). Speciation was calculated from dissolved TM concentrations and DOC concentrations for ambient pH and temperatures. pH value was calculated from total alkalinity and the partial pressure of CO_2 (pCO_2) using CO2SYS (*74*). Total alkalinity was determined by Gran titration (Apollo, Scitech) on samples collected using the CTD frame equipped with standard Niskin bottles following protocols described in (*75*). pCO_2 was measured continuously in surface waters using an equilibration chamber interfaced to an infrared gas analyzer (LICOR instruments, LI-820) that was connected to the ship's seawater supply as described in (*76*). Speciation calculations are described in more detail in Supplementary Text.

SUPPLEMENTARY MATERIALS

Supplementary material for this article is available at https://science.org/doi/10.1126/sciadv.abm2249

REFERENCES AND NOTES

1. P. Friedlingstein, M. O'Sullivan, M. W. Jones, R. M. Andrew, J. Hauck, A. Olsen, G. P. Peters, W. Peters, J. Pongratz, S. Sitch, C. le Quéré, J. G. Canadell, P. Ciais, R. B. Jackson, S. Alin, L. E. O. C. Aragão, A. Arneth, V. Arora, N. R. Bates, M. Becker, A. Benoit-Cattin, H. C. Bittig, L. Bopp, S. Bultan, N. Chandra, F. Chevallier, L. P. Chini, W. Evans, L. Florentie, P. M. Forster, T. Gasser, M. Gehlen, D. Gilfillan, T. Gkritzalis, L. Gregor, N. Gruber, I. Harris, K. Hartung, V. Haverd, R. A. Houghton, T. Ilyina, A. K. Jain, E. Joetzjer, K. Kadono, E. Kato, V. Kitidis, J. I. Korsbakken, P. Landschützer, N. Lefèvre, A. Lenton, S. Lienert, Z. Liu, D. Lombardozzi, G. Marland, N. Metzl, D. R. Munro, J. E. M. S. Nabel, S. I. Nakaoka, Y. Niwa, K. O'Brien, T. Ono, P. I. Palmer, D. Pierrot, B. Poulter, L. Resplandy, E. Robertson, C. Rödenbeck, J. Schwinger, R. Séférian, I. Skjelvan, A. J. P. Smith, A. J. Sutton, T. Tanhua, P. P. Tans, H. Tian, B. Tilbrook, G. van der Werf, N. Vuichard, A. P. Walker, R. Wanninkhof, A. J. Watson, D. Willis, A. J. Wiltshire, W. Yuan, X. Yue, S. Zaehle, Global carbon budget 2020. *Earth Syst. Sci. Data* **12**, 3269–3340 (2020).
2. S. Roshan, T. DeVries, Efficient dissolved organic carbon production and export in the oligotrophic ocean. *Nat. Comm.* **8**, 1–8 (2017).
3. D. A. Hansell, C. A. Carlson, *Biogeochemistry of Marine Dissolved Organic Matter* (Elsevier, ed. 2, 2015).
4. E. J. Zakem, N. M. Levine, Systematic variation in marine dissolved organic matter stoichiometry and remineralization ratios as a function of lability. *Global Biogeochem. Cycles* **33**, 1389–1407 (2019).
5. K. B. Ksionzek, O. J. Lechtenfeld, S. L. McCallister, P. Schmitt-Kopplin, J. K. Geuer, W. Geibert, B. P. Koch, Dissolved organic sulfur in the ocean: Biogeochemistry of a petagram inventory. *Science* **354**, 456–459 (2016).
6. K. B. Ksionzek, J. Zhang, K.-U. Ludwichowski, D. Wilhelms-Dick, S. Trimborn, T. Jendrossek, G. Kattner, B. P. Koch, Stoichiometry, polarity, and organometallics in solid-phase extracted dissolved organic matter of the Elbe-Weser estuary. *PLOS ONE* **13**, e0203260 (2018).
7. M. Gledhill, K. N. Buck, The organic complexation of iron in the marine environment: A review. *Front. Microbiol.* **3**, 69 (2012).
8. F. L. L. Muller, Exploring the potential role of terrestrially derived humic substances in the marine biogeochemistry of iron. *Front. Earth Sci.* **6**, 1–20 (2018).
9. J. E. Jacquot, J. W. Moffett, Copper distribution and speciation across the International GEOTRACES Section GA03. *Deep-Sea Res. Part II: Top. Stud. Oceanogr.* **116**, 187–207 (2015).
10. J. R. Donat, K. A. Lao, K. W. Bruland, Speciation of dissolved copper and nickel in South San Francisco Bay: A multi-method approach. *Anal. Chim. Acta* **284**, 547–571 (1994).
11. R. M. Boiteau, C. P. Till, A. Ruacho, R. M. Bundy, N. J. Hawco, A. M. McKenna, K. A. Barbeau, K. W. Bruland, M. A. Saito, D. J. Repeta, Structural characterization of natural nickel and copper binding ligands along the US GEOTRACES Eastern Pacific Zonal Transect. *Front. Mar. Sci.* **3**, 243 (2016).
12. K. W. Bruland, Complexation of zinc by natural organic ligands in the central North Pacific. *Limnol. Oceanogr.* **34**, 269–285 (1989).
13. C. M. G. van den Berg, A. G. Merks, E. K. Duursma, Organic complexation and its control of the dissolved concentrations of copper and zinc in the Scheldt estuary. *Estuar. Coast. Shelf Sci.* **24**, 785–797 (1987).
14. M. A. Saito, J. W. Moffett, Complexation of cobalt by natural organic ligands in the Sargasso Sea as determined by a new high-sensitivity electrochemical cobalt speciation method suitable for open ocean work. *Mar. Chem.* **75**, 49–68 (2001).
15. A. E. Noble, D. C. Ohnemus, N. J. Hawco, P. J. Lam, M. A. Saito, Coastal sources, sinks and strong organic complexation of dissolved cobalt within the US North Atlantic GEOTRACES transect GA03. *Biogeosciences* **14**, 2715–2739 (2017).
16. H. Zhang, C. M. G. van den Berg, R. Wollast, The determination of interactions of cobalt(II) with organic compounds in seawater using cathodic stripping voltammetry. *Mar. Chem.* **28**, 285–300 (1990).
17. V. E. Oldham, A. Mucci, B. M. Tebo, G. W. Luther, Soluble Mn(III)–L complexes are abundant in oxygenated waters and stabilized by humic ligands. *Geoch. Cosmochim. Acta.* **199**, 238–246 (2017).
18. X. Liu, F. J. Millero, The solubility of iron hydroxide in sodium chloride solutions. *Geochim. Cosmochim. Acta* **63**, 3487–3497 (1999).

19. K. Zhu, M. J. Hopwood, J. E. Groenenberg, A. Engel, E. P. Achterberg, M. Gledhill, Influence of pH and dissolved organic matter on iron speciation and apparent iron solubility in the peruvian shelf and slope region. *Environ. Sci. Technol.* **55**, 9372–9383 (2021).
20. H. Irving, R. J. P. Williams, The stability of transition-metal complexes. *J. Chem. Soc.* **3245**, 3192–3210 (1953).
21. R. G. Pearson, Absolute electronegativity and hardness: Application to inorganic chemistry. *Inorg. Chem.* **27**, 734–740 (1988).
22. D. R. Turner, M. Whitfield, A. G. Dickson, The equilibrium speciation of dissolved components in freswater and seawater at 25°C at 1 atm. pressure. *Geochim. Cosmochim. Acta* **45**, 855–882 (1981).
23. R. T. Powell, A. Wilson-Finelli, Importance of organic Fe complexing ligands in the Mississippi River plume. *Est. Coast. Shelf Sci.* **58**, 757–763 (2003).
24. R. Krachler, R. F. Krachler, G. Wallner, S. Hann, M. Laux, M. F. Cervantes Recalde, F. Jirsa, E. Neubauer, F. von der Kammer, T. Hofmann, B. K. Keppler, River-derived humic substances as iron chelators in seawater. *Mar. Chem.* **174**, 85–93 (2015).
25. E. R. Sholkovitz, E. A. Boyle, N. B. Price, The removal of dissolved humic acids and iron during estuarine mixing. *Earth Plan. Sci. Lett.* **40**, 130–136 (1978).
26. R. Yang, H. Su, S. Qu, X. Wang, Capacity of humic substances to complex with iron at different salinities in the Yangtze River estuary and East China Sea. *Sci. Rep.* **7**, 1–9 (2017).
27. A. Körtzinger, A significant CO_2 sink in the tropical Atlantic Ocean associated with the Amazon River plume. *Geophys. Res. Lett.* **30**, 2287 (2003).
28. Y.-C. Liang, M.-H. Lo, C.-W. Lan, H. Seo, C. C. Ummenhofer, S. Yeager, R.-J. Wu, J. D. Steffen, Amplified seasonal cycle in hydroclimate over the Amazon river basin and its plume region. *Nature Comm.* **11**, 1–11 (2020).
29. M. Seidel, P. L. Yager, N. D. Ward, E. J. Carpenter, H. R. Gomes, A. V. Krusche, J. E. Richey, T. Dittmar, P. M. Medeiros, Molecular-level changes of dissolved organic matter along the Amazon River-to-ocean continuum. *Mar. Chem.* **177**, 218–231 (2015).
30. A. P. Hollister, H. Whitby, M. Seidel, P. Lodeiro, M. Gledhill, A. Koschinsky, Dissolved concentrations and organic speciation of copper in the Amazon River estuary and mixing plume. *Mar. Chem.* **234**, 104005 (2021).
31. L. M. de Carvalho, A. P. Hollister, C. Trindade, M. Gledhill, A. Koschinsky, Distribution and size fractionation of nickel and cobalt species along the Amazon estuary and mixing plume. *Mar. Chem.* **236**, 104019 (2021).
32. E. A. Boyle, S. S. Huested, B. Grant, The chemical mass balance of the Amazon plume—II. Copper, nickel, and cadmium. *Deep-Sea Res. I Oceanogr. Res. Pap.* **29**, 1355–1364 (1982).
33. M. Van Hulten, R. Middag, J. C. Dutay, H. De Baar, M. Roy-Barman, M. Gehlen, A. Tagliabue, A. Sterl, Manganese in the west Atlantic Ocean in the context of the first global ocean circulation model of manganese. *Biogeosciences* **14**, 1123–1152 (2017).
34. M. J. A. Rijkenberg, R. Middag, P. Laan, L. J. A. Gerringa, H. M. van Aken, V. Schoemann, J. T. M. de Jong, H. J. W. de Baar, The distribution of dissolved iron in the West Atlantic Ocean. *PLOS ONE* **9**, e101323 (2014).
35. L. M. Mosley, P. S. Liss, Particle aggregation, pH changes and metal behaviour during estuarine mixing: Review and integration. *Mar. Freshw. Res.* **71**, 300–310 (2020).
36. C. J. Milne, D. G. Kinniburgh, W. H. van Riemsdijk, E. Tipping, Generic NICA–Donnan model parameters for metal-ion binding by humic substances. *Environ. Sci. Technol.* **37**, 958–971 (2003).
37. T. Spiegel, P. Vosteen, K. Wallmann, S. A. L. Paul, M. Gledhill, F. Scholz, Updated estimates of sedimentary potassium sequestration and phosphorus release on the Amazon shelf. *Chem. Geol.* **560**, 120017 (2021).
38. T. Dittmar, N. Hertkorn, G. Kattner, R. J. Lara, Mangroves, a major source of dissolved organic carbon to the oceans. *Global Biogeochem. Cycles* **20**, GB1012 (2006).
39. A. Cabral, T. Dittmar, M. Call, J. Scholten, C. E. Rezende, N. E. Asp, M. Gledhill, M. Seidel, I. R. Santos, Carbon and alkalinity outwelling off Amazon mangroves across the groundwater-creek-shelf continuum. *Limnol. Oceanogr. Lett.* **6**, 369–378 (2021).
40. T. Dittmar, B. Koch, N. Hertkorn, G. Kattner, A simple and efficient method for the solid-phase extraction of dissolved organic matter (SPE-DOM) from seawater. *Limnol. Oceanogr. Meth.* **6**, 230–235 (2008).
41. H. Waska, A. Koschinsky, M. J. Ruiz Chancho, T. Dittmar, Investigating the potential of solid-phase extraction and Fourier-transform ion cyclotron resonance mass spectrometry (FT-ICR-MS) for the isolation and identification of dissolved metal–Organic complexes from natural waters. *Mar. Chem.* **173**, 78–92 (2015).
42. M. Voss, E. Asmala, I. Bartl, J. Carstensen, D. J. Conley, J. W. Dippner, C. Humborg, K. Lukkari, J. Petkuviene, H. Reader, C. Stedmon, I. Vybernaite-Lubiene, N. Wannicke, M. Zilius, Origin and fate of dissolved organic matter in four shallow Baltic Sea estuaries. *Biogeochemistry* **154**, 1–19 (2020).
43. C. Lønborg, X. A. Álvarez-Salgado, S. Duggan, C. Carreira, Organic matter bioavailability in tropical coastal waters: The great barrier reef. *Limnol. Oceanogr.* **63**, 1015–1035 (2018).
44. E. Mawji, M. Gledhill, J. A. Milton, G. A. Tarran, S. Ussher, A. Thompson, G. A. Wolff, P. J. Worsfold, E. P. Achterberg, Hydroxamate siderophores: Occurrence and importance in the Atlantic Ocean. *Environ. Sci. Technol.* **42**, 8675–8680 (2008).
45. M. Gledhill, K. Zhu, D. Rusiecka, E. P. Achterberg, Competitive interactions between microbial siderophores and humic-like binding sites in european shelf sea waters. *Front. Mar. Sci.* **9**, 595 (2022).
46. C. Mori, I. R. Santos, H.-J. Brumsack, B. Schnetger, T. Dittmar, M. Seidel, Non-conservative behavior of dissolved organic matter and trace metals (Mn, Fe, Ba) driven by porewater exchange in a subtropical mangrove-estuary. *Front. Mar. Sci.* **6**, 481 (2019).
47. P. B. Kozelka, K. W. Bruland, Chemical speciation of dissolved Cu, Zn, Cd, Pb in Narragansett Bay, Rhode Island. *Mar. Chem.* **60**, 267–282 (1998).
48. M. M. Abualhaija, H. Whitby, C. M. G. van den Berg, Competition between copper and iron for humic ligands in estuarine waters. *Mar. Chem.* **172**, 46–56 (2015).
49. K. N. Buck, M. C. Lohan, C. J. M. Berger, K. W. Bruland, Dissolved iron speciation in two distinct river plumes and an estuary: Implications for riverine iron supply. *Limnol. Oceanogr.* **52**, 843–855 (2007).
50. A. Turner, M. Martino, Modelling the equilibrium speciation of nickel in the Tweed Estuary, UK: Voltammetric determinations and simulations using WHAM. *Mar. Chem.* **102**, 198–207 (2006).
51. C. M. G. van den Berg, M. Nimmo, Determination of interactions of nickel with dissolved organic material in seawater using cathodic stripping voltammetry. *Sci. Total Environ.* **60**, 185–195 (1987).
52. J. L. Weishaar, G. R. Aiken, B. A. Bergamaschi, M. S. Fram, R. Fujii, K. Mopper, Evaluation of specific ultraviolet absorbance as an indicator of the chemical composition and reactivity of dissolved organic carbon. *Environ. Sci. Technol.* **37**, 4702–4708 (2003).
53. O. J. Lechtenfeld, B. P. Koch, W. Geibert, K. U. Ludwichowski, G. Kattner, Inorganics in organics: Quantification of organic phosphorus and sulfur and trace element speciation in natural organic matter using HPLC-ICPMS. *Anal. Chem.* **83**, 8968–8974 (2011).
54. T. Y. Ho, A. Quigg, Z. V. Finkel, A. J. Milligan, K. Wyman, P. G. Falkowski, F. M. M. Morel, The elemental composition of some marine phytoplankton. *J. Phycol.* **39**, 1145–1159 (2003).
55. A. M. Pohlabeln, G. V. Gomez-Saez, B. E. Noriega-Ortega, T. Dittmar, Experimental evidence for abiotic sulfurization of marine dissolved organic matter. *Front. Mar. Sci.* **4**, 364 (2017).
56. C. S. Hopkinson Jr., J. J. Vallino, Efficient export of carbon to the deep ocean through dissolved organic matter. *Nature* **433**, 142–145 (2005).
57. D. J. DeMaster, R. C. Aller, Biogeocghemical processes on the Amazon Shelf: Changes in dissolved and particulate fluxes during river/ocean mixing, in *The Biogeochemistry of the Amazon Basin*, M. E. McClain, R. L. Victoria, J. E. Richey, Eds. (Oxford Univ. Press, 2001), pp. 328–357.
58. A. Rathgeb, T. Causon, R. Krachler, S. Hann, Determination of size-dependent metal distribution in dissolved organic matter by SEC-UV/VIS-ICP-MS with special focus on changes in seawater. *Electrophoresis* **37**, 1063–1071 (2016).
59. L. M. Laglera, C. M. G. van den Berg, Evidence for geochemical control of iron by humic substances in seawater. *Limnol. Oceanogr.* **54**, 610–619 (2009).
60. C. Sukekava, J. Downes, H. A. Slagter, L. J. A. Gerringa, L. M. Laglera, Determination of the contribution of humic substances to iron complexation in seawater by catalytic cathodic stripping voltammetry. *Talanta* **189**, 359–364 (2018).
61. M. Oss, A. Kruve, K. Herodes, I. Leito, Electrospray ionization efficiency scale of organic compounds. *Anal. Chem.* **82**, 2865–2872 (2010).
62. A. M. Pohlabeln, T. Dittmar, Novel insights into the molecular structure of non-volatile marine dissolved organic sulfur. *Mar. Chem.* **168**, 86–94 (2015).
63. P. Lodeiro, C. Rey-Castro, C. David, J. Puy, E. P. Achterberg, M. Gledhill, Seasonal variations in proton binding characteristics of dissolved organic matter isolated from the southwest Baltic Sea. *Environ. Sci. Technol.* **55**, 16215–16223 (2021).
64. P. Lodeiro, C. Rey-Castro, C. David, E. P. Achterberg, J. Puy, M. Gledhill, Acid-base properties of dissolved organic matter extracted from the marine environment. *Sci. Total Environ.* **729**, 138437 (2020).
65. Z. V. Finkel, J. Beardall, K. J. Flynn, A. Quigg, T. A. V. Rees, J. A. Raven, Phytoplankton in a changing world: Cell size and elemental stoichiometry. *J. Plankton Res.* **32**, 119–137 (2010).
66. J. Zhang, G. Kattner, B. P. Koch, Interactions of trace elements and organic ligands in seawater and implications for quantifying biogeochemical dynamics: A review. *Earth Sci. Rev.* **192**, 631–649 (2019).
67. L. K. Koopal, T. Saito, J. P. Pinheiro, W. H. van Riemsdijk, Ion binding to natural organic matter: General considerations and the NICA–Donnan model. *Colloids Surf. A Physicochem. Eng. Asp.* **265**, 40–54 (2005).
68. T. Hiemstra, W. H. van Riemsdijk, Biogeochemical speciation of Fe in ocean water. *Mar. Chem.* **102**, 181–197 (2006).
69. E. Gensac, J. M. Martinez, V. Vantrepotte, E. J. Anthony, Seasonal and inter-annual dynamics of suspended sediment at the mouth of the Amazon River: The role of continental and oceanic forcing, and implications for coastal geomorphology and mud bank formation. *Cont. Shelf Res.* **118**, 49–62 (2016).
70. W. G. Sunda, S. A. Huntsman, Microbial oxidation of manganese in a North Carolina estuary. *Limnol. Oceanogr.* **32**, 552–564 (1987).

71. J. W. Moffett, J. Ho, Oxidation of cobalt and manganese in seawater via a common microbially catalyzed pathway. *Geochim. Cosmochim. Acta* **60**, 3415–3424 (1996).
72. A. E. Noble, C. H. Lamborg, D. C. Ohnemus, P. J. Lam, T. J. Goepfert, C. I. Measures, C. H. Frame, K. L. Casciotti, G. R. DiTullio, J. Jennings, M. A. Saito, Basin-scale inputs of cobalt, iron, and manganese from the Benguela-Angola front to the South Atlantic Ocean. *Limnol. Oceanogr.* **57**, 989–1010 (2012).
73. J. C. L. Meeussen, Orchestra: An object-oriented framework for implementing chemical equilibrium models. *Environ. Sci. Technol.* **37**, 1175–1182 (2003).
74. D. Pierrot, E. Lewis, D. W. R. Wallace, MS Excel program developed for CO_2 system calculations (U.S. Department of Energy, 2006).
75. A. G. Dickson, The carbonate system in seawater: Equilibrium chemistry and measurements, in *Guide to Best Practices for Ocean Acidification Research and Data Reporting*, U. Riebesell, V. J. Fabry, L. Hansson, J. P. Gattuso, Eds. (European Commission, 2010), pp. 17–41.
76. H. O. Sawakuchi, V. Neu, N. D. Ward, M. de L. C. Barros, A. M. Valerio, W. Gagne-Maynard, A. C. Cunha, D. F. S. Less, J. E. M. Diniz, D. C. Brito, A. V. Krusche, J. E. Richey, Carbon dioxide emissions along the lower amazon river. *Front. Mar. Sci.* **4**, 76 (2017).
77. J. A. Hawkes, P. J. R. Sjöberg, J. Bergquist, L. J. Tranvik, Complexity of dissolved organic matter in the molecular size dimension: Insights from coupled size exclusion chromatography electrospray ionisation mass spectrometry. *Faraday Discuss.* **218**, 52–71 (2019).
78. R Development Core Team, *R: A Language and Environment for Statistical Computing* (R Foundation for Statistical Computing, 2016); {ISBN} 3–900051–07-0, 10.1038/sj.hdy.6800737.
79. D. Kessner, M. Chambers, R. Burke, D. Agus, P. Mallick, ProteoWizard: Open source software for rapid proteomics tools development. *Bioinformatics* **24**, 2534–2536 (2008).
80. T. Pluskal, S. Castillo, A. Villar-Briones, M. Orešič, MZmine 2: Modular framework for processing, visualizing, and analyzing mass spectrometry-based molecular profile data. *BMC Bioinform.* **11**, 1–11 (2010).
81. S. K. Schum, L. E. Brown, L. R. Mazzoleni, MFAssignR: Molecular formula assignment software for ultrahigh resolution mass spectrometry analysis of environmental complex mixtures. *Environ. Res.* **191**, 110114 (2020).
82. G. Cutter, K. Casciotti, P. Croot, W. Geibert, L.-E. Heimburger, M. C. Lohan, H. Planquette, T. van de Flierdt, Sampling and Sample-handling Protocols for GEOTRACES Cruises Version 3 (GEOTRACES International Project Office, 2017), pp. 139.
83. B. O. Keller, J. Sui, A. B. Young, R. M. Whittal, Interferences and contaminants encountered in modern mass spectrometry. *Anal. Chim. Acta* **627**, 71–81 (2008).
84. C. J. Milne, D. G. Kinniburgh, E. Tipping, Generic NICA-Donnan model parameters for proton binding by humic substances. *Environ. Sci. Technol.* **35**, 2049–2059 (2001).
85. M. F. Benedetti, W. H. van Riemsdijk, L. K. Koopal, Humic substances considered as a heterogeneous donnan gel phase. *Environ. Sci. Technol.* **30**, 1805–1813 (1996).
86. M. Gledhill, E. P. Achterberg, K. Li, K. N. Mohamed, M. J. A. Rijkenberg, Influence of ocean acidification on the complexation of iron and copper by organic ligands in estuarine waters. *Mar. Chem.* **177**, 421–433 (2015).
87. K. Zhu, A. J. Birchill, A. Milne, S. J. Ussher, M. P. Humphreys, N. Carr, C. Mahaffey, M. C. Lohan, E. P. Achterberg, M. Gledhill, Equilibrium calculations of iron speciation and apparent iron solubility in the Celtic Sea at ambient pH using the NICA-Donnan model. *Mar. Chem.* **237**, 104038 (2021).
88. P. M. Williams, Organic and inorganic constituents of the amazon river. *Nature* **218**, 937–938 (1968).
89. J. M. Smoak, J. M. Krest, P. W. Swarzenski, Geochemistry of the Amazon Estuary, in *Estuaries*, P. J. Wangersky, Ed. (Springer, 2005), pp. 71–90.
90. R. Chester, *Marine Geochemistry* (Chapman & Hall, 1990).
91. B. P. Koch, M. R. Witt, R. Engbrodt, T. Dittmar, G. Kattner, Molecular formulae of marine and terrigenous dissolved organic matter detected by electrospray ionization Fourier transform ion cyclotron resonance mass spectrometry. *Geochim. Cosmochim. Acta* **69**, 3299–3308 (2005).
92. R. M. Smith, A. E. Martell, R. J. Motekaitis, NIST critically selected stability constants of metal complexes database (NIST Standard Reference Database 46, 2004), pp. 22.

Acknowledgments: We thank the captain and crew of RV *Meteor* for help and support during the cruise. We thank V. Neu (ISARH, Universidade Federal Rural da Amazônia) for supplying the CO_2 analyzer and P. Lodeiro and T. Spiegel for assistance with sampling. We thank A. Mutzberg for the nutrient analysis, K. Nachtigall for HPLC analysis of chlorophyll a, M. Martinez for alkalinity analysis, and T. Steffens and D. Jasinski for assistance with HPLC-ESI/ICP-MS analysis. We thank the Brazilian government (Ministério da Marinha) for the opportunity to sample in the Brazilian exclusive economic zone (EEZ). **Funding:** This work was funded by German Research Foundation grant GL 807/2-1, German Research Foundation grant KO 2906/13-1, and German Research Foundation Cluster of Excellence (390741603) Helmholtz Association. **Author contributions:** Conceptualization: M.G. Methodology: M.G., T.D., and A.K. Investigation: M.G., A.H., M.S., and K.Z. Resources: M.G., A.K., E.P.A., and T.D. Writing (original draft): M.G., A.H., M.S., and A.K. Writing (review and editing): M.G., A.H., M.S., K.Z., E.P.A., T.D., and A.K. **Competing interests:** The authors declare that they have no competing interests. **Data and materials availability:** All data needed to evaluate the conclusions in the paper are present in the paper and/or the Supplementary Materials. Additional data related to this paper is available in Pangaea (doi: https://doi.pangaea.de/10.1594/PANGAEA.941455).

Submitted 2 February 2022
Accepted 22 June 2022
Published 5 August 2022
10.1126/sciadv.abm2249

ScienceAdvances

Trace metal stoichiometry of dissolved organic matter in the Amazon plume

Martha GledhillAdrienne HollisterMichael SeidelKechen ZhuEric P. AchterbergThorsten DittmarAndrea Koschinsky

Sci. Adv., 8 (31), eabm2249. • DOI: 10.1126/sciadv.abm2249

Science Advances (ISSN) is published by the American Association for the Advancement of Science. 1200 New York Avenue NW, Washington, DC 20005. The title *Science Advances* is a registered trademark of AAAS.